Mon. Not. R. Astron. Soc. **385,** 1511–1522 (2008) doi:10.1111/j.1365-2966.2008.12927.x

Probing the intrinsic shape and alignment of dark matter haloes using SDSS galaxy groups

Yougang Wang,[1,8⋆] Xiaohu Yang,[2,3] H. J. Mo,[4] Cheng Li[2,3,5,6], Frank C. van den Bosch,[7] Zuhui Fan[8] and Xuelei Chen[1]

[1]*National Astronomical Observatories, Chinese Academy of Sciences, Beijing 100012, China*
[2]*Shanghai Astronomical Observatory (SHAO), the Partner Group of MPA, Nandan Road 80, Shanghai 200030, China*
[3]*Joint Institute for Galaxy and Cosmology (JOINGC) of Shanghai Astronomical Observatory and University of Science and Technology of China*
[4]*Department of Astronomy, University of Massachusetts, Amherst MA 01003-9305*
[5]*Max-Planck-Institut für Astrophysik, Karl-Schwarzschild-Strasse 1, 85748 Garching, Germany*
[6]*Centre for Astrophysics, University of Science and Technology of China (USTC), Hefei, Anhui 230026, China*
[7]*Max-Planck Institute for Astronomy, Königstuhl 17, D-69117 Heidelberg, Germany*
[8]*Department of Astronomy, Peking University, Beijing 100871, China*

Accepted 2008 January 7. Received 2008 January 5; in original form 2007 October 13

ABSTRACT

We study the three-dimensional and projected shapes of galaxy groups in the Sloan Digital Sky Survey Data Release 4, and examine the alignment between the orientation of the central galaxy and the spatial distribution of satellite galaxies. The projected ellipticity of a group is measured using the moments of the discrete distribution of its member galaxies. We infer the three-dimensional and projected axis ratios of their dark matter haloes by comparing the measured ellipticity distributions with those obtained from Monte Carlo simulations of projected, triaxial dark matter haloes with different axis ratios. We find that the halo shape has a strong dependence on the halo mass. While the haloes of low-mass groups are nearly spherical, those of massive groups tend to be prolate. For groups containing at least four members, the statistical distribution of their measured ellipticities does not have a strong dependence on the colours of their central galaxies. Our analysis further shows that the average three-dimensional axis ratio for haloes with $12 < \log[M/(h^{-1}\,\mathrm{M}_{\odot})] \leqslant 15$ is about $1:0.46:0.46$, resulting in a projected axis ratio of $\sim$0.77. Our results for the alignment between the orientation of the central galaxy of a group and the distribution of their satellite galaxies are in broad agreement with those obtained by Yang et al. The distribution of satellite galaxies preferentially aligns with the major axis of the central galaxy, with a clear dependence on both halo mass and galaxy colours. In particular, the alignment is stronger in more massive groups, and the strongest alignment is seen between red centrals and the distribution of red satellites. For groups with blue centrals, no significant alignment is detected. Finally, we examine how the observed alignment can be reproduced with the information about the halo axis ratios. The observed alignment signal can be reproduced if the angle between the major axis of the central galaxy and the projected major axis of the host halo has a Gaussian distribution with a mean of 0° and a dispersion of $\sim 23^{\circ}$. This dispersion is larger for groups with blue centrals than those with red centrals.

Key words: methods: statistical – galaxies: haloes – galaxies: structure – dark matter – large-scale structure of Universe.

1 INTRODUCTION

In the cold dark matter (CDM) scenario, small dark matter haloes form first and grow subsequently to larger structures via accretion and merging processes. Such processes are generally anisotropic so that dark matter haloes are expected to be non-spherical. The orientations of dark matter haloes can be related to their surrounding structures, such as filaments and large-scale walls (e.g. Faltenbacher et al. 2002; Einasto et al. 2003; Avila-Reese et al. 2005; Hopkins, Bahcall & Bode 2005; Kasun & Evrard 2005; Altay, Colberg Jörg & Croft 2006; Basilakos et al. 2006; Aragon-Calvo et al. 2007;

⋆E-mail: wangyg@bao.ac.cn

Hahn et al. 2007a,b; Maulbetsch et al. 2007; Ragone-Figueroa & Plionis 2007). The last major merger of a dark matter halo may play an important role in determining its shape (van Haarlem & van de Weygaert 1993), although interactions between the gas and the dark matter components are also expected to play a role (Kazantzidis et al. 2004). Thus, the shapes and orientations of dark matter haloes contain abundant information about their formation histories, which, in turn depend on the underlying cosmology (Ho, Bahcall & Bode 2006; Lee 2006). On the other hand, the non-sphericity of dark matter haloes can also lead to systematic errors in cosmological studies (Sulkanen 1999; Wang & Fan 2006). Therefore, it is of great importance to characterize the shapes of dark matter haloes, both observationally and theoretically.

The shapes of clusters of galaxies can be probed using X-ray observations, studies of the Sunyaev–Zeldovich effect and gravitational lensing (e.g. Zaroubi et al. 1998; Reblinsky 2000; Zaroubi et al. 2001; Lee & Suto 2004; Wang & Fan 2004; De Filippis et al. 2005; Sereno et al. 2006). However, one can also use the spatial distribution of satellite galaxies, since these are expected to be good tracers of the shapes of their host haloes. The large redshift surveys carried out in recent years, for example, the 2dF Galaxy Redshift Survey (2dFGRS) and Sloan Digital Sky Survey (SDSS), have provided angular positions and redshifts for hundreds of thousands of galaxies, which allow detailed studies of the shapes of large samples and the shape dependence on richness, multiplicity and dynamical evolution of groups and clusters. Early studies preferred the prolate shapes (Carter & Metcalfe 1980; Plionis, Barrow & Frenk 1991; Fasano et al. 1993; Basilakos, Plionis & Maddox 2000; Cooray 2000; Orlov, Petrova & Martynova 2001), but did not exclude the oblate solutions. Plionis, Basilakos & Tovmassian (2004, hereafter P04) estimated the shape distribution of the Updated Zwicky Catalogue–Southern Sky Redshift Survey (UZC-SSRS2) groups of galaxies by analysing the spatial distribution of group members. They found that the prolate-like shape fits very well the cosmic structure on a large scale apart from the disc galaxy. Somewhat surprisingly, they also found that poor groups are more elongated than rich ones, results which are opposite to what is found in numerical simulations (e.g. Kasun & Evrard 2005; Allgood et al. 2006).

Somewhat surprisingly, these results are opposite to what is found with numerical simulations (Kasun & Evrard 2005; Allgood et al. 2006). Recently, they estimated the average group morphology of the Percolation-Inferred Galaxy Group (2PIGG) and found that the prolate or triaxial with pronounced prolate shapes are the only acceptable morphological model (Plionis, Basilakos & Ragone-Figueroa 2006).

In this paper, we use data from the SDSS to study the shapes of galaxy groups, under the assumption that the spatial distribution of group members traces the matter distributions of their underlying dark matter haloes. Differing from previous studies, we run Monte Carlo simulations to generate the same number of member galaxies as in each of the observed groups under the assumption that haloes of the groups follow the triaxial model of Jing & Suto (2002, hereafter JS02). We then make two-dimensional projected distributions of these member galaxies, which serve as our Monte Carlo mock samples. We compare the ellipticity distribution obtained from the mock sample with the observed one to extract information on the axis ratios of dark matter haloes.

In the second part of this paper, we revisit the alignment between the spatial distribution of satellite galaxies in groups and the orientation of their central galaxies (hereafter 'centrals'). It is important to assess accurately the alignment of the dark matter halo because it holds important clues regarding the actual assembled history of dark matter haloes. Extensive studies with high-resolution simulations have shown dark matter haloes have anisotropic distributions of subhaloes that are aligned with their major axis (Knebe et al. 2004; Libeskind et al. 2005; Wang et al. 2005; Zentner et al. 2005). This anisotropy mainly owes to a preferred direction of satellite accretion along large-scale filaments (Tormen 1997; Vitvitska et al. 2002; Aubert, Pichon & Colombi 2004; Knebe et al. 2004; Wang et al. 2005; Zentner et al. 2005). In addition, the tidal forces from the host halo may also induce new alignments (e.g. Ciotti & Dutta 1994; Usami & Fujimoto 1997; Fleck & Kuhn 2003; Wang et al., in preparation). Conversely, some non-linear effects such as violent relaxation and encounters can weaken the primordial alignment (e.g. Porciani, Dekel & Hoffman 2002).

Comparing with the simulation studies, the observational search for a possible alignment of centrals and their satellites has a long and confusing history. The first study of such an alignment was by Holmberg (1969), who found that satellites are preferentially located along the minor axes of isolated disc galaxies. Holmberg's study was restricted to projected satellite-central distances of $r_{\rm p} \lesssim 50\,{\rm kpc}$. Subsequent studies, however, were unable to confirm this so-called 'Holmberg effect' (Hawley & Peebles 1975; Sharp, Lin & White 1979; MacGillivray et al. 1982). Zaritsky et al. (1997) studied the distribution of satellites around spiral hosts, and were also unable to detect any significant alignment for $r_{\rm p} \lesssim 200\,{\rm kpc}$, but they found a preferred minor-axis alignment for $300\,{\rm kpc} \lesssim r_{\rm p} \lesssim 500\,{\rm kpc}$. Our Milky Way and M31 have satellites that lie in great planes that are highly inclined to their discs (Lynden-Bell 1976, 1982; Majewski 1994; Hartwick 1996, 2000; Kroupa, Theis & Boily 2005; Koch & Grebel 2006; McConnachie & Irwin 2006; Metz, Kroupa & Jerjen 2007). With large redshift surveys, such as 2dFGRS and SDSS, much larger samples of galaxy groups can be used to discuss the alignment problem. Sales & Lambas (2004) used a set of 1498 host galaxies with 3079 satellites from the 2dFGRS, and found a large-scale alignment of the satellites along the host minor axes for $300\,{\rm kpc} \lesssim r_{\rm p} \lesssim 500\,{\rm kpc}$. Brainerd (2005) studied a sample of isolated SDSS galaxies and found that the distribution of satellite galaxies is strongly aligned with the major axis of the disc host galaxy. Yang et al. (2006, hereafter Y06), using a galaxy group catalogue similar to the one used here, but based on the SDSS Data Release 2 (DR2), studied the alignment signal as function of the colours of the central and satellite galaxies. They found that the alignment strength is strongest between red centrals and red satellites, while the satellite distribution in systems with a blue central is consistent with being isotropic. Y06 also found that the alignment strength is stronger in more massive haloes and at smaller projected radii from the central. These results have subsequently been confirmed by several independent studies (Agustsson & Brainerd 2006a; Donoso, O'Mill & Lambas 2006; Agustsson & Brainerd 2007; Azzaro et al. 2007). Using the same group catalogue as that used here, Faltenbacher et al. (2007a) examined several additional alignment signals. They found that the orientations of red satellites are preferentially aligned radially in the direction of the brightest group galaxies (BGG). In addition, they found a weak but significant indication that the orientations of satellite galaxies are directly aligned with that of their BGG. Comparing with the earlier studies of the alignment between brightest cluster galaxies (BCGs) and their parent clusters (Carter & Metcalfe 1980; Binggeli 1982; Struble 1990; West 1994; Kim et al. 2001), Faltenbacher et al. (2007a) have given more detailed results for the large samples. These various detections of alignment between centrals and satellites have triggered a number of investigations into the connection between the shapes and orientations

of dark matter haloes and their galaxy population, with the goal to improve our understanding of the formation of dark matter haloes and galaxies (e.g. Agustsson & Brainerd 2006b, hereafter, AB06; Brunino et al. 2007; Faltenbacher et al. 2007b; Kang et al. 2007, hereafter K07; Pereira, Bryan & Gill 2007; Sales et al. 2007).

In addition to measuring the alignment signals from the SDSS observations for groups of different masses, we try to infer the correlation between the orientations of the central and that of its host halo, statistically but both from the observations. If the projected orientation of a central is perfectly aligned with the projected orientation of its host dark matter halo, assuming that satellite galaxies trace the matter distribution, the alignment signal between the distribution of satellite galaxies and the orientation of their central is strongest. By comparing the alignment signals measured from the observations and the Monte Carlo samples, we can estimate the deviation (misalignment angle) of the orientation of central from the orientation of its host dark matter halo. We use a Gaussian distribution function to quantify this misalignment angle.

This paper is organized as follows. In Section 2, we briefly describe the observational data used for this study. Section 3 presents our measurements of the intrinsic shapes of dark matter haloes, where the three-dimensional and two-dimensional axis ratios are determined using Monte Carlo simulations. Section 4 shows the alignment signal we measured from the SDSS and its implication for the shape correlation between the centrals and the dark matter haloes. Finally, Section 5 presents a summary and discussion. Throughout this paper, we refer to the inferred shape from the satellite galaxy distribution as the shape of the group and the corresponding dark matter halo, and use the major-axis direction of the satellite distribution to indicate the orientation of the group and the corresponding dark matter halo.

2 DATA

The analysis presented in this paper is based on the SDSS DR4 galaxy group catalogue of Yang et al. (2007). This group catalogue is constructed applying the halo-based group finder of Yang et al. (2005a) to the New York University Value-Added Galaxy Catalogue (NYU-VAGC; see Blanton et al. 2005), which is based on SDSS DR4 (Adelman-McCarthy et al. 2006). From this catalogue, Yang et al. selected all galaxies in the main Galaxy sample with redshifts in the range $0.01 \leqslant z \leqslant 0.20$ and with a redshift completeness $\mathcal{C} > 0.7$. This sample of galaxies is used to construct three group samples: sample I, which only uses the 362 356 galaxies with measured redshifts from the SDSS, sample II which also includes 7091 galaxies with SDSS photometry but with redshifts taken from alternative surveys and sample III which includes an additional 38 672 galaxies that lack a redshift due to fiber collisions, but which we assign the redshift of its nearest neighbour (cf. Zehavi et al. 2002). The present analysis is based on sample II which consists of 369 447 galaxies distributed over 301 237 groups with a sky coverage of 4514 deg^2. Details of the group finder and the general properties of the groups can be found in Yang et al. (2007).

In this paper, the central is defined to be the brightest galaxy in the group and other galaxies are satellites. We also take the most massive (in terms of stellar mass) group member as the central. As we have tested, the difference between these two definitions is too small to be noted. The group masses are estimated using the ranking of group's characteristic luminosity, $L_{19.5}$, defined as the combined luminosity of all group members with ${}^{0.1}M_r - 5\log h \leqslant -19.5$. More details of the mass estimations can be found in Yang et al. (2007). Note that the selected galaxy groups contain a small fraction of interlopers, that is, false members assigned to a group. If the distribution of these interlopers is uncorrelated (or anticorrelated) with that of the true members of the group, our results on both the ellipticity and the alignment can be biased. According to Yang et al. (2005a, 2007), the average fraction of interlopers in the group is less than 20 per cent. We have tested the effect of such fraction by assuming that the distribution of the interlopers is uncorrelated with the shape of the group and is spherical, we find that the presence of the interlopers can decrease the ellipticity of the groups and the alignment signals by $\sim$10 per cent.

Note that in these group catalogues survey edge effects have been taken into account (Yang et al. 2007). Only groups with $f_{\rm edge} \geqslant 0.6$ are selected, where $1 - f_{\rm edge}$ is the fraction of galaxies in a group that are missed due to the edge effects. In order to obtain the ellipticity distribution of galaxy groups, we only use groups with at least four members (one central and at least three satellites), which results in a catalogue of 5184 groups. However, in studying the alignment between satellite galaxies and the orientation of their centrals, we enlarge our sample by using all groups with at least two members (one central and one satellite). This sample gives a total of 62 212 unique central-satellite pairs, many more than in the DR2 sample used by Y06.

3 THE INTRINSIC SHAPE OF THE DARK MATTER HALO

3.1 Methodology

We now describe how we use the satellite distribution to determine the ellipticity distribution of galaxy groups and their corresponding dark matter haloes. The observed satellite distribution in a group suffers from severe discreteness effects. In particular, since each group contains only a small number of galaxies, there is a high level of Poisson noise in the determination of the ellipticity based on its galaxy distribution. Thus, the ellipticity directly measured can only be used as a rough indicator of the underlying, true ellipticity. We will use mock samples to quantify how the observed ellipticity distribution is related to the real distribution. Assuming that the distribution of satellite galaxies in a group traces the mass distribution in the corresponding dark matter halo, we can infer, in a statistical sense, the shapes of dark matter haloes from the observed distribution of the group ellipticities. In order to obtain the principal axes and the orientation of a group projected on the sky, we define the inertia tensor as

$$X_{ij} = \sum_{i=1}^{n} x_{i,n} x_{j,n}, \tag{1}$$

where $(x_{i,n}, x_{j,n})$ are the projected coordinates (with the central at the origin) of the nth satellite galaxy. The semimajor and semiminor axes of the ellipse, L_a and L_b (two roots of the following equation), can be derived by solving the equation:

$$\begin{vmatrix} X_{11} - L^2 & X_{12} \\ X_{12} & X_{22} - L^2 \end{vmatrix} = 0. \tag{2}$$

The direction of the major axis is given by the eigenvector $\boldsymbol{r} = [1, (L_a^2 - X_{11})/X_{12}]$, while the ellipticity, ϵ, and the axis ratio, η, are

$$\epsilon = 1 - L_b/L_a \quad \text{and} \quad \eta = L_b/L_a. \tag{3}$$

Throughout this paper, we use the ellipticity ϵ and axis ratio η to refer to the quantities *measured directly* from the data. The inferred shapes of the underlying dark matter haloes are described either by their two-dimensional or three-dimensional axis ratios.

As mentioned above, to quantify the true shapes of the dark matter haloes associated with the galaxy groups, one needs to construct mock samples that include the same selection effects. We construct Monte Carlo SDSS DR4 group catalogues as follows. First, we determine the number of satellites for each of the SDSS groups. Secondly, we re-distribute these satellites according to a spherical NFW profile (Navarro, Frenk & White 1996, 1997) or a triaxial profile by JS02. Thirdly, we project the three-dimensional distribution of satellite galaxies on to a two-dimensional plane and measure the ellipticity, $\epsilon_{\rm MC}$, for each Monte Carlo group. Such Monte Carlo approach was firstly introduced by Basilakos et al. (2000) to recover the projected cluster ellipticity distribution and the true projected ellipticity distribution taking into account the background and discreetness effects (see also Plionis et al. 2006). 30 Monte Carlo realizations are generated and we estimate the average and scatter of the ellipticity distribution using these 30 Monte Carlo samples. Some small groups with masses smaller than $10^{11.6}\,h^{-1}\,{\rm M}_{\odot}$, where SDSS DR4 group catalogue does not provide mass estimates, are removed from our sample.

The first model for the mass profile used in our Monte Carlo simulations is a spherical NFW density profile,

$$\rho_{\rm NFW}(r) = \frac{\rho_0 \delta_c}{(r/r_{\rm s})(1+r/r_{\rm s})^2}, \tag{4}$$

where ρ_0 is the average mass density of the universe, $r_{\rm s}$ is a scale radius and $\delta_c = 200c^3/3[\ln(1+c) - c/(1+c)]$. The concentration parameter c is defined as $c = r_{200}/r_{\rm s}$, with r_{200} the radius within which the mean density is 200 times the average mass density of the universe. This model is fully determined for a halo of a given mass (or, equivalently, r_{200}) once the concentration parameter is given. The concentration parameter depends on the halo mass M and redshift z, for which we use the model of Bullock et al. (2001):

$$c(M,z) = \frac{c_\star}{1+z}\left(\frac{M}{10^{14}h^{-1}\,{\rm M}_{\odot}}\right)^{-0.13}, \tag{5}$$

where $c_\star = 8$, as is appropriate for the ΛCDM model.

The other density profile we use is that proposed by JS02. Using high-resolution numerical simulations, JS02 proposed an NFW-like triaxial density profile for dark matter haloes, which has the form

$$\rho(R)_{\rm JS02} = \frac{\rho_0 \delta_c}{(R/R_0)^{\alpha}(1+R/R_0)^{3-\alpha}}, \tag{6}$$

where $R = a(x^2/a^2 + y^2/b^2 + z^2/c^2)^{1/2}$, and $a \geqslant b \geqslant c$ are the lengths of the three principal semiaxes. For the value of α, it is found that both $\alpha = 1$ and 1.5 can provide a good fit to the simulated profiles. Detailed comparisons showed that $\alpha = 1$ is slightly better for cluster-scale haloes, while $\alpha = 1.5$ gives better fit for galactic haloes (JS02). Therefore, we adopt $\alpha = 1.5$ for groups with masses smaller than $10^{13}\,h^{-1}\,{\rm M}_{\odot}$, and $\alpha = 1.0$ for more massive groups (In fact, the results are not sensitive to the value of α adopted. We have also adopted $\alpha = 1.0$ for all groups, their differences are tiny.).

3.2 Ellipticity distribution

Figs 1 and 2 show the probability distributions of the ellipticity obtained from the SDSS DR4 (dotted histogram) and from the Monte Carlo simulations (solid histogram with errorbars). In Fig. 1, we assume that the distribution of satellite galaxies follows a spherical NFW profile, while in Fig. 2 we assume that the distribution of satellite galaxies follows the JS02 model. For the JS02 triaxial distribution, we have adopted the model parameters (axis ratios and concentrations) given in JS02. In both cases, we randomly select a line-of-sight direction, project the three-dimensional satellite distribution on to a two-dimensional plane and measure the ellipticity distribution using the method outlined above. In each plot, the parameter N represents the lower limit on the number of galaxies in each group (including the central). Note that the ellipticity distribution is strongly dependent on this lower limit, with poorer groups being more elongated. The mean ellipticity increases from ∼0.40 for groups with richness $N \geqslant 10$ to ∼0.54 for groups with $N \geqslant 4$. However, this does not mean that the true halo shape is more elongated for poorer groups; the trend is largely a result of the discrete sampling. For example, in the extreme case where only one satellite galaxy is observed, the measured ellipticity will always be unity regardless of the shape of the underlying dark matter halo. Thus, the shape of the underlying halo shape can only be probed in an indirect way, i.e. by comparing the observed distribution with that of the Monte Carlo samples.

From Figs 1 and 2, it appears that the triaxial model of JS02 fits the data better relative to the spherical NFW model.

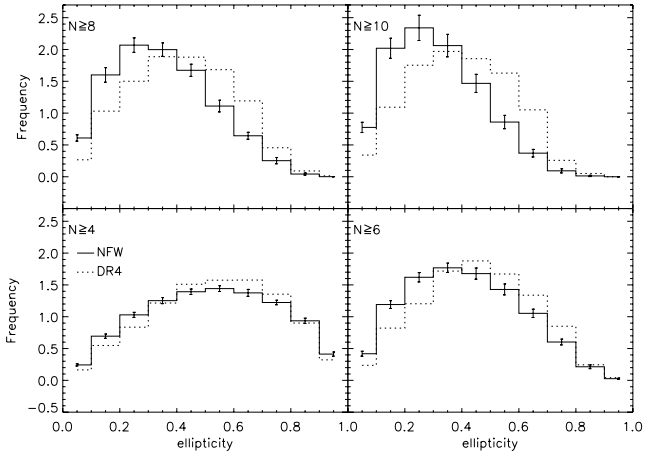

Figure 1. Probability distributions of the ellipticity in the SDSS DR4 (dotted histogram) and Monte Carlo re-samplings (solid histogram with errorbars). Here, we assume that the distribution of satellite galaxies in groups follows a spherical NFW profile.

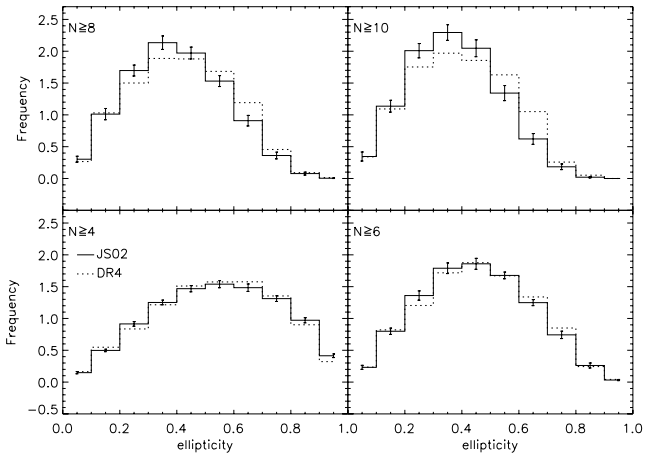

Figure 2. Same as Fig. 1, but here we assume that the satellite galaxies are distributed in groups according to JS02 triaxial model.

3.3 The three-dimensional and projected shapes of dark matter haloes

Numerous studies have used numerical *N*-body simulations to probe the non-spherical shapes of dark matter haloes as traced by dark matter particles (e.g. JS02; Kazantzidis et al. 2004) or by subhaloes (e.g. Diemand, Moore & Stadel 2004). The subhaloes are more closely associated with satellite galaxies, which have been found to be biased tracers of the mass distribution. There is a negative spatial bias at the centre, and a corresponding positive velocity bias. It is still unclear whether this reflects numerical artefact (i.e. overmerging), or whether this is real. Yang et al. (2005b) studied the satellite distributions in the 2dFGRS groups and found evidence that the number density distribution of satellites is less concentrated than expected dark matter. Here, we probe the mean values of axis ratios of dark matter haloes as traced by SDSS galaxies. For this purpose, we first divide the SDSS DR4 groups into subsamples according to their halo masses, and measure the corresponding ellipticity distribution as traced by the satellite galaxies. Then, using the model of JS02 with given axis ratios, we construct 30 realizations of Monte Carlo simulations and measure the corresponding ellipticity distributions. By changing model parameters (i.e. axis ratios) so that the predicted ellipticity distributions match the observed one, we determine the underlying axis ratios of dark matter haloes. Here, the comparison between model predictions and observation is done in terms of a χ^2, defined as

$$\chi^2 = \sum_{i=1}^{N_b} \frac{(\langle f_{i(\mathrm{MC})}\rangle - f_{i(\mathrm{obs})})^2}{\sigma^2[f_{i(\mathrm{MC})}]}, \tag{7}$$

where $N_b = 10$ denotes the bin number of the ellipticity distribution. $\langle f_{i(\mathrm{MC})}\rangle$ and $\sigma^2(f_{i(\mathrm{MC})})$ are, respectively, the average amplitude and 1σ deviation of the ellipticity distributions obtained from the 30 realizations of Monte Carlo simulations, while $f_{i(\mathrm{obs})}$ is the amplitude of the ellipticity distribution obtained from the SDSS groups. Note that for each set of axis ratios, $\sigma^2[f_{i(\mathrm{MC})}]$ changes slightly. However, as we have tested, using constant $\sigma^2[f_{i(\mathrm{MC})}]$ does not have a significant impact on our measurement of the best-fitting axis ratios. Thus, we use $\sigma^2[f_{i(\mathrm{MC})}]$ computed from the 30 Monte Carlo simulations and estimate the best-fitting axial ratios by minimizing the χ^2. Here, the minimization is performed on the regular 100×100 (three-dimensional) or 100 (two-dimensional) axis ratio grids.

In Fig. 3, we compare the ellipticity distribution for groups in different mass bins (dotted histograms) with those of the best-fitting Monte Carlo simulation (solid histograms with errorbars). The corresponding best fit, three-dimensional axis ratios for the dark matter haloes are listed in the second column of Table 1. As one can see, the three-dimensional axis ratios recovered are different for groups with different richness. The results indicate that less massive haloes are more spherical, while more massive haloes tend to be more prolate.

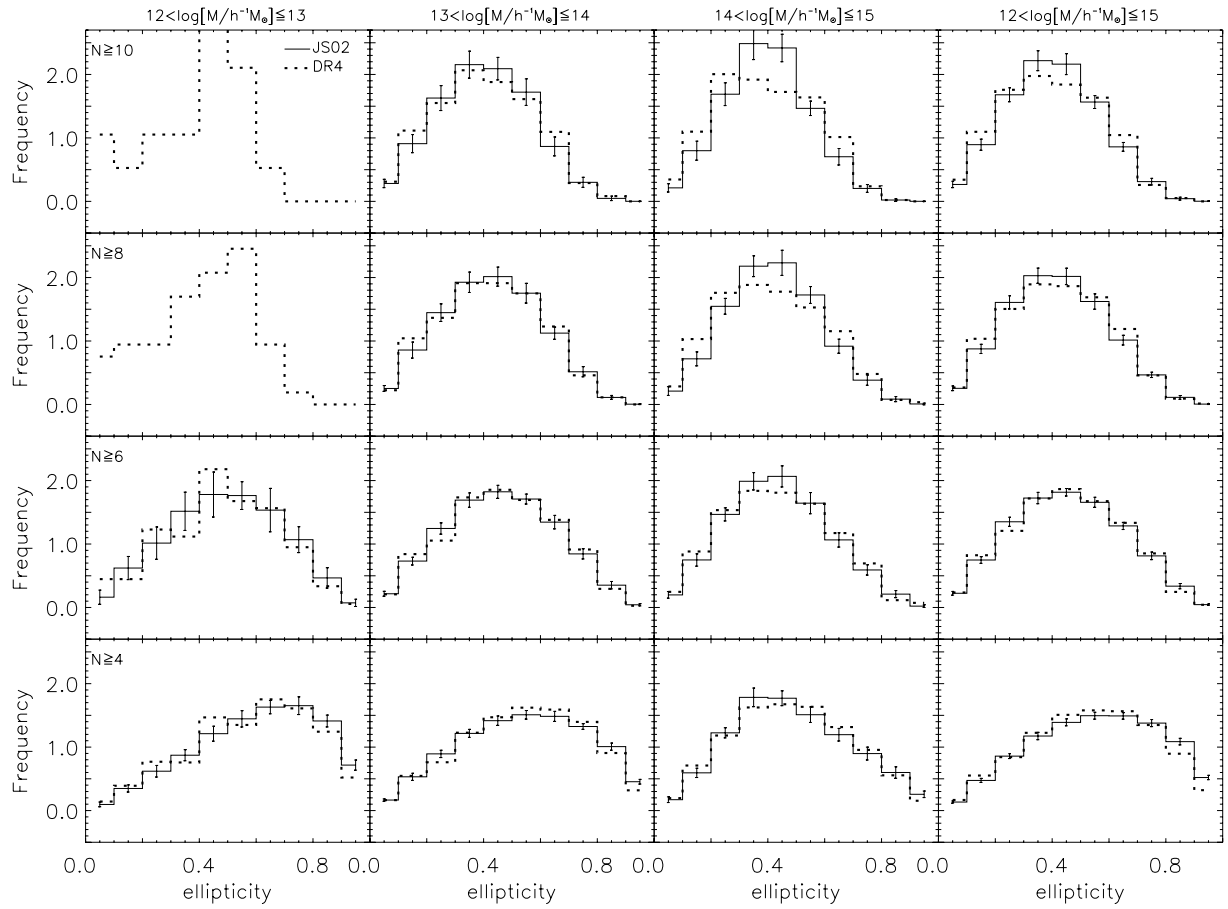

Figure 3. Similar to Fig. 1, but for groups in different mass bins as indicated on top of the panels. In this plot, the Monte Carlo simulations are performed according to the JS02 profile with the best-fitting three-dimensional axis ratios. The line-of-sight (projection) direction is random.

Table 1. Best-fitting parameters for groups in different halo mass bins. From top to bottom, values are listed for groups with different members $N \geqslant 4$, 6, 8 and 10, respectively.

Mass bin	Three-dimensional axis ratios (I)	χ^2 (I)	Two-dimensional axis ratios (II)	χ^2 (II)
$12 < M' \leqslant 13^a$	1:0.96:0.85	22.58	$0.96^{+0.01}_{-0.02}$	46.16
$13 < M' \leqslant 14$	1:0.80:0.72	29.93	$0.83^{+0.02}_{-0.01}$	28.30
$14 < M' \leqslant 15$	1:0.88:0.44	11.86	$0.69^{+0.01}_{-0.01}$	19.13
$12 < M' \leqslant 15$	1:0.46:0.46	67.63	$0.77^{+0.03}_{-0.01}$	56.02
$12 < M' \leqslant 13$	1:0.96:0.95	12.47	$0.86^{+0.02}_{-0.04}$	20.49
$13 < M' \leqslant 14$	1:0.96:0.63	10.75	$0.76^{+0.01}_{-0.01}$	16.29
$14 < M' \leqslant 15$	1:0.35:0.35	17.78	$0.68^{+0.01}_{-0.01}$	52.10
$12 < M' \leqslant 15$	1:0.51:0.48	13.17	$0.72^{+0.01}_{-0.01}$	14.63
$12 < M' \leqslant 13^b$	–	–	–	–
$13 < M' \leqslant 14$	1:0.87:0.53	5.36	$0.72^{+0.01}_{-0.01}$	10.40
$14 < M' \leqslant 15$	1:0.33:0.33	33.19	$0.70^{+0.01}_{-0.02}$	89.14
$12 < M' \leqslant 15$	1:0.43:0.43	17.05	$0.72^{+0.01}_{-0.01}$	29.53
$12 < M' \leqslant 13$	–	–	–	–
$13 < M' \leqslant 14$	1:0.84:0.50	7.68	$0.72^{+0.01}_{-0.01}$	12.63
$14 < M' \leqslant 15$	1:0.61:0.36	34.84	$0.68^{+0.01}_{-0.01}$	60.24
$12 < M' \leqslant 15$	1:0.39:0.39	23.04	$0.71^{+0.01}_{-0.01}$	48.66

[a] $M' = \log [M/(h^{-1}\,\mathrm{M}_\odot)]$.
[b] The axis ratios in the $12 < M' \leqslant 13$ mass bin with $N \geqslant 8$ and 10 are absent because our group sample contains too few of these rich groups for a reliable measurement of the ellipticity distribution.

These results are in good agreement with Paz et al. (2006; hereafter P06), who studied the shapes of dark matter haloes, both projected in three-dimensional, using simulations and groups constructed from the 2dFGRS (Colless et al. 2001) and the SDSS DR3.

In addition to the three-dimensional axis ratios, we can also look into the projected two-dimensional axis ratios. Assuming a projected major-to-minor axis ratio, we re-sample the sky positions of satellite galaxies in each group in a Monte Carlo way, and measure the corresponding ellipticity distribution for groups of different masses and richness. Here again, by changing the two-dimensional axis ratio, we can obtain the one that best matches the observed ellipticity distribution of groups. The results are shown in Fig. 4, and the corresponding best fit, two-dimensional axis ratios are listed in the fourth column of Table 1. Once again less massive groups are found be more spherical. Note that groups in the same mass bin, but with different richness, have only slightly different two-dimensional axis ratios.

The χ^2 values presented in Table 1 for the best-fitting models are quite large, especially for groups with halo masses 10^{12}–$10^{15}\,h^{-1}\,\mathrm{M}_\odot$ in the three-dimensional cases, and in a few two-dimensional cases. Possible reasons for such large χ^2 are: (i) the assumption of a constant axis ratio is not accurate to describe the shape of the groups and (ii) the shapes of observed groups do not follow a Gaussian distribution. Unfortunately, without better knowledge about these issues, it is difficult to come up with a better model.

Observationally, only gravitational lensing data can directly probe the two-dimensional, projected mass distribution of dark matter haloes. However, at the present time, such observations are limited in both quality and quantity (see Hoekstra, Yee & Gladders 2004; Mandelbaum et al. 2006). For clusters of galaxies, additional data are available from X-ray data and from studies of the Sunyaev–Zeldovich effect. These data yield constraints on the shapes of cluster haloes from their gas distribution. Mohr et al. (1995) used a sample of 57 X-ray clusters observed by the Einstein telescope and obtained a mean two-dimensional axis ratio, $\langle\eta\rangle = 0.80$, and a dispersion $\sigma_\eta = 0.12$. With the JS02 model, Wang & Fan (2004) studied the Sunyaev–Zeldovich effect and X-ray surface brightness profiles for clusters of galaxies. Based on a sample of clusters with masses above $M_{\rm lim} = 10^{14}\,h^{-1}\,\mathrm{M}_\odot$, they found that the average axis ratios are $\langle\eta\rangle \sim 0.84$. Sereno et al. (2006) used a sample of 25 X-ray selected clusters observed by *Chandra* and *XMM–Newton*, and obtained a mean-projected axis ratio $\langle\eta\rangle = 0.80 \pm 0.02$. Recently, Flores et al. (2007) predicted that the mean axis ratio is $\langle\eta\rangle = 0.82$ and a scatter is $\sigma_\eta = 0.09$ using a simple analytical model. Note, though, that all these measurements are for the axis ratios of the hot intracluster gas. Lee & Suto (2003) presented an analytical expression that links the ellipticity of the gas to that of the dark matter halo, assuming that the intracluster gas is in hydrostatic equilibrium. Although this relation is obtained in three-dimensional, we assume that it is also valid for the two-dimensional distributions. By converting the axis ratio of the gas distribution into the dark matter distribution using the results in fig. 3 of Lee & Suto (2003), we infer two-dimensional axis ratios for dark matter haloes of 0.6 ± 0.1, in good agreement with our measurements (0.69 for groups with halo masses 10^{14}–$10^{15}\,h^{-1}\,\mathrm{M}_\odot$).

3.4 Dependence of halo shape on the colour of centrals

The colour–magnitude relation of galaxies is found to have a bimodal distribution, consisting of a red 'sequence' and a blue 'cloud' (e.g. Baldry et al. 2004; Li et al. 2006). In this section, we test whether haloes that host red or blue centrals have different shapes

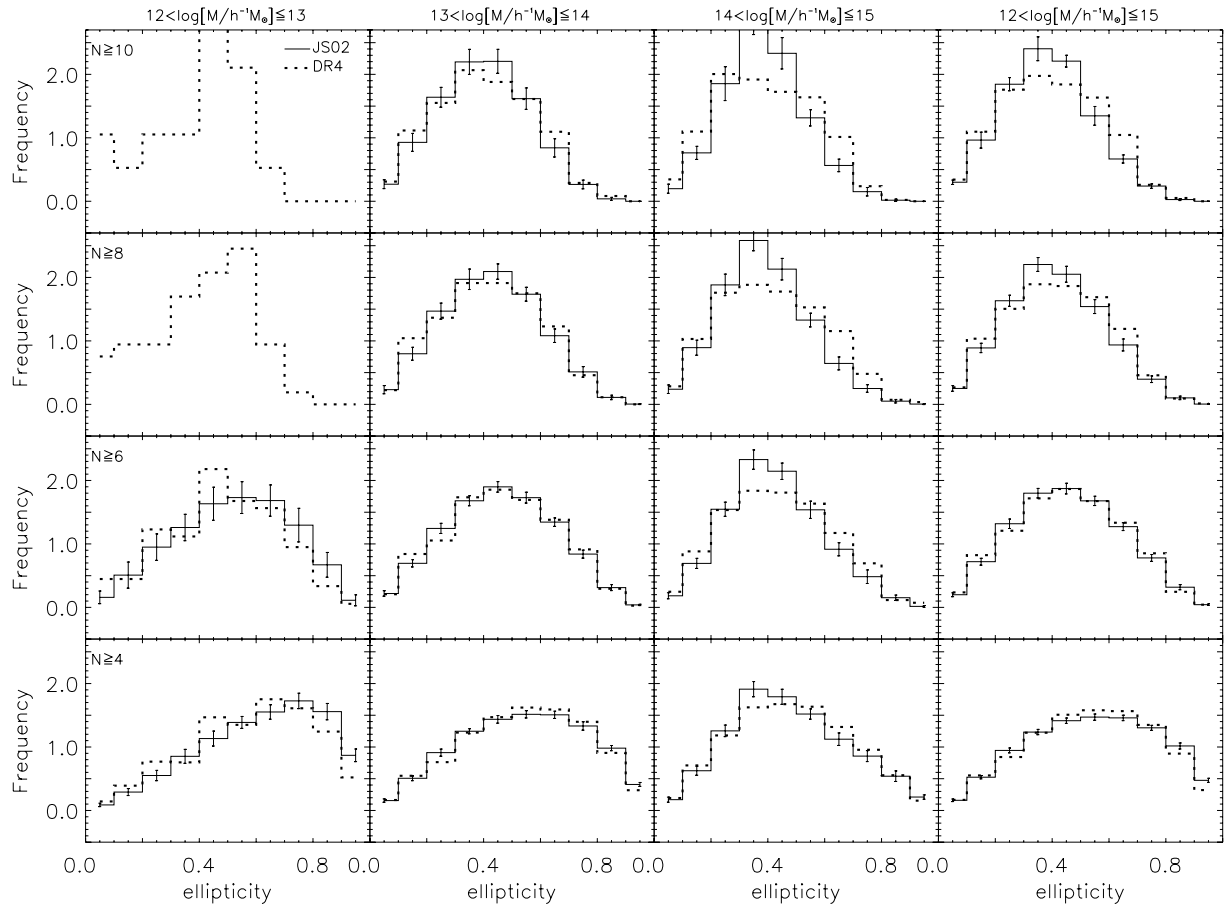

Figure 4. Similar to Fig. 3, but for the best-fitting two-dimensional axis ratios.

(the motivation behind this will become clear in Section 4). Following Li et al. (2006) and Yang, Mo & van den Bosch (2008), we separate galaxies into red and blue population using the following dividing curve:

$$^{0.1}(g-r)_0 = 1.022 - 0.0651 * M_{r,23} - 0.00311 * M_{r,23}^2, \qquad (8)$$

where $M_{r,23} = {}^{0.1}M_r - 5\log h + 23$, and ${}^{0.1}M_r - 5\log h$ is the absolute magnitude $K + E$ corrected to $z = 0.1$ using the method described in Blanton et al. (2003). We define galaxies with $^{0.1}(g-r) \geqslant {}^{0.1}(g-r)_0$ as red galaxies and the rest as blue galaxies. Here, $^{0.1}(g-r)$ is the colour in the SDSS g and r bands $K + E$ corrected to $z = 0.1$. In Fig. 5, we compare the ellipticity distribution for groups with red and blue centrals. The results indicate that there is no significant difference between the shape of groups with blue or red centrals.

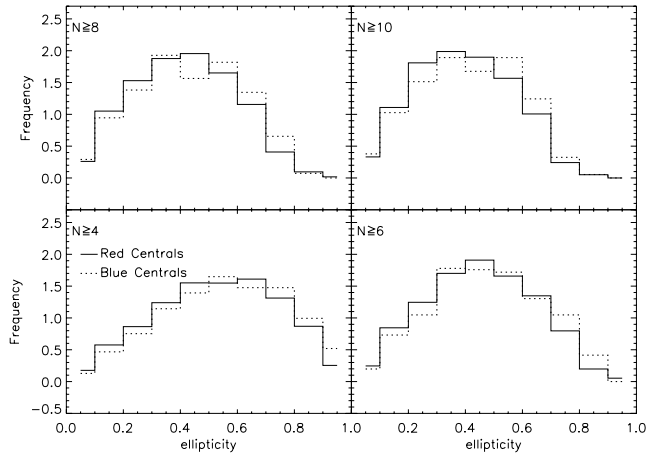

Figure 5. Probability distribution of the ellipticity for groups with different centrals: red (solid line) versus blue (dotted line).

4 ALIGNMENT BETWEEN CENTRALS AND DARK MATTER HALOES

4.1 Quantifying the alignment

In order to quantify the distribution of satellite galaxies in groups relative to the orientations of their centrals, we follow Brainerd (2005) and compute the distribution function, $P(\theta)$, where θ is the angle between the major axis of the central group galaxy and the direction of a satellite relative to the central. The angle θ is constrained in the range $0^\circ \leqslant \theta \leqslant 90^\circ$, where $\theta = 0^\circ$ (90°) implies that the satellite lies along the major (minor) axis of the central. The orientation of the central is based on the isophotal position angle in the r band, as given in the SDSS-DR4 (Adelman-McCarthy et al. 2006). We have checked the distribution of these position angles and found it to be isotropic.

For a given set of central and satellite galaxies, we first count the total number of central-satellite pairs, $N(\theta)$, for a number of bins in θ. Next, we construct 100 random samples in which we randomize

the orientations of all centrals, and compute $\langle N_{\rm R}(\theta)\rangle$, the average number of central-satellite pairs as function of θ. Note that this ensures that the random samples have exactly the same selection effects as the real sample, so that any significant difference between $N(\theta)$ and $N_{\rm R}(\theta)$ reflects a genuine alignment between the orientations of the centrals and the distributions of their corresponding satellite galaxies.

To quantify the strength of any possible alignment, we follow Y06 and define the distribution of normalized pair counts:

$$f_{\rm pairs}(\theta) = \frac{N(\theta)}{\langle N_{\rm R}(\theta)\rangle}. \quad (9)$$

Note that in the absence of any alignment, $f_{\rm pairs}(\theta) = 1$, while $f_{\rm pairs}(\theta) > 1$ at small θ implies a satellite distribution with a preferred alignment along the major axis of their central. We use $\sigma_{\rm R}(\theta)/\langle N_{\rm R}(\theta)\rangle$, where $\sigma_{\rm R}$ is the standard deviation of $N_{\rm R}(\theta)$ obtained from the 100 random samples, to assess the significance of the deviation of $f_{\rm pairs}(\theta)$ from unity. In addition to this normalized pair count, we also compute the average angle $\langle\theta\rangle$. In the absence of any alignment $\langle\theta\rangle = 45^\circ$, however, $\langle\theta\rangle = 45^\circ$ does not mean an isotropic distribution. Major and minor axis alignments are characterized by $\langle\theta\rangle < 45^\circ$ and $\langle\theta\rangle > 45^\circ$, respectively. The significance of any alignment can be expressed in terms of σ_θ, the variance in $\langle\theta\rangle_{\rm R}$, which is obtained from the 100 random samples.

Fig. 6 shows $f_{\rm pairs}(\theta)$ for all central-satellite pairs (solid line) in our SDSS group catalogue. Clearly, $f_{\rm pairs}(\theta) > 1$ for small θ indicating that satellite galaxies are distributed preferentially along the major axis of their central. This is also evident from the fact that $\langle\theta\rangle = 42.^\circ46 \pm 0.^\circ12$, which deviates from the case of no alignment (i.e. $\langle\theta\rangle = 45^\circ$) by almost 21σ! For comparison, using a group catalogue constructed from the SDSS DR2 data by Weinmann et al. (2006), similar to that used here, Y06 found $\langle\theta\rangle = 42.^\circ2 \pm 0.^\circ2$, in excellent agreement with the results presented here. Note, though, that the statistical error presented here is much smaller, due to the larger group catalogue used. The existence of alignment owns in part to the non-spherical distribution of the satellite galaxies in dark matter haloes (e.g. Kang et al. 2005, K07; Libeskind et al. 2005; Zentner et al. 2005; AB06), which has been used in the previous section to probe the overall shapes of the dark matter mass distribution. For comparison, the dotted lines in Fig. 6 show $f_{\rm pairs}(\theta)$ for groups with at least four members. The resulting alignment signal is slightly stronger than for the full sample (which includes all central-satellite pairs in groups with at least two members). This is consistent with the fact that (i) groups with more satellites are more massive and (ii) more massive groups are less spherical (see also Section 4.1.2 below).

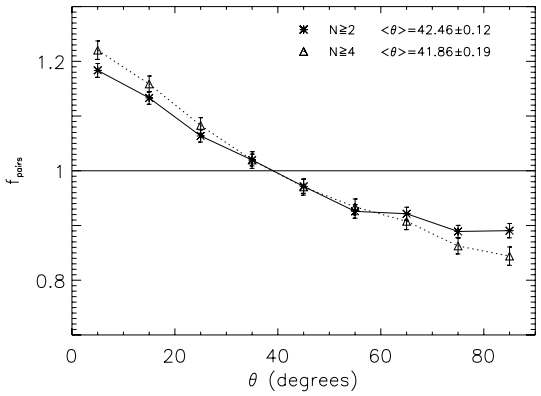

Figure 6. The normalized probability distribution, $f_{\rm pairs}(\theta)$, of the angle θ between the major axis of the central and the direction connecting the satellite galaxy and the central. Results are measured for groups with at least two members (solid line) and four members (dotted line).

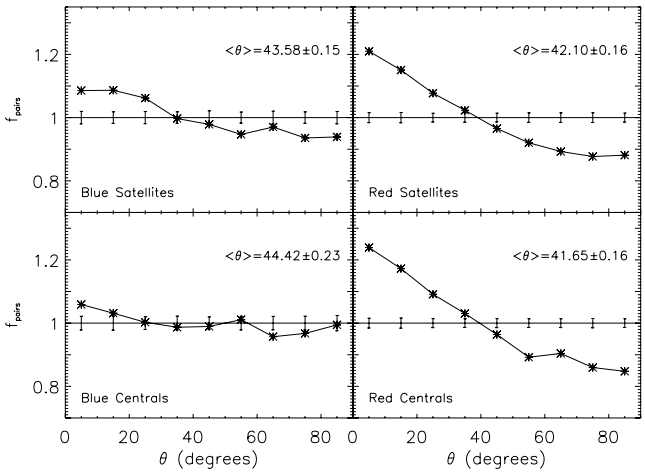

Figure 7. Same as Fig. 6, but for different subsamples of central-satellite pairs, separated according to the $^{0.1}(g-r)$ colours either for satellite galaxies (upper two panels) and for centrals (lower two panels).

4.1.1 *Dependence on galaxy colour*

In order to study how the alignment depends on various properties of the central and satellite galaxies, we follow Y06 and divide our sample of central-satellite pairs into different subsamples. The upper panels of Fig. 7 show the alignment signals obtained for blue and red satellites, while the lower panels show the results for blue and red centrals. As one can see, there is a strong dependence on the colours of both the centrals and satellites. In particular, groups with red centrals and red satellites show a stronger alignment than those with blue centrals and blue satellites, in good agreement with previous studies (Y06; Agustsson & Brainerd 2007; Azzaro et al. 2007). As pointed out by K07, groups with blue centrals tend to have slightly more interlopers, which may cause an artificial reduction of their measured alignment. However, even after this is corrected for groups with blue centrals still show a weak alignment.

In Fig. 8, we show the alignment, $f_{\rm pairs}(\theta)$, for the four colour combinations of centrals and satellites. As one can see pairs between blue centrals and blue satellites do not show any alignment, while pairs between red centrals and red satellites show the strongest alignment. Pairs between red centrals and blue satellites and pairs between blue centrals and red satellites show alignment with intermediate strength. All these findings are in excellent agreement with, and more significant than, those obtained in Y06.

4.1.2 *Dependence on halo mass*

Fig. 9 shows the alignment measure for groups of different halo masses. From the upper panels, one can see that the alignment is stronger for more massive groups. We also examine the mass dependence of the alignment separately for groups with blue and red centrals, the results of which are shown in the middle and lower panels of Fig. 9, respectively. The alignment is quite different for blue and red centrals. For all halo masses probed here, red centrals reveal a much stronger alignment with their satellite galaxies than blue centrals. In fact, except for the most massive haloes with

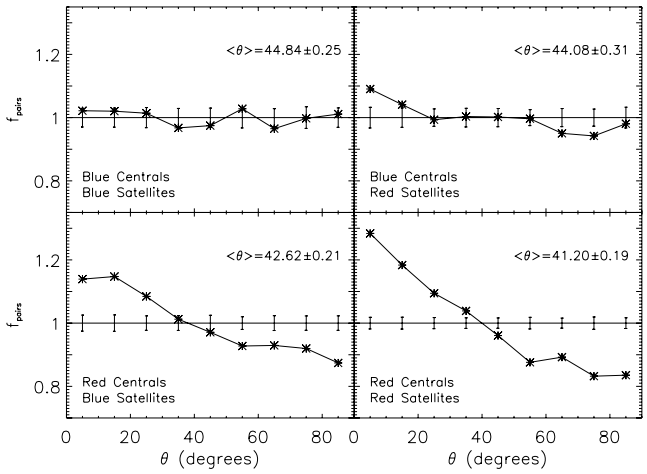

Figure 8. Same as Fig. 7, except that here we split the sample according to different combinations of the colours for *both* central and the satellite galaxies, as indicated.

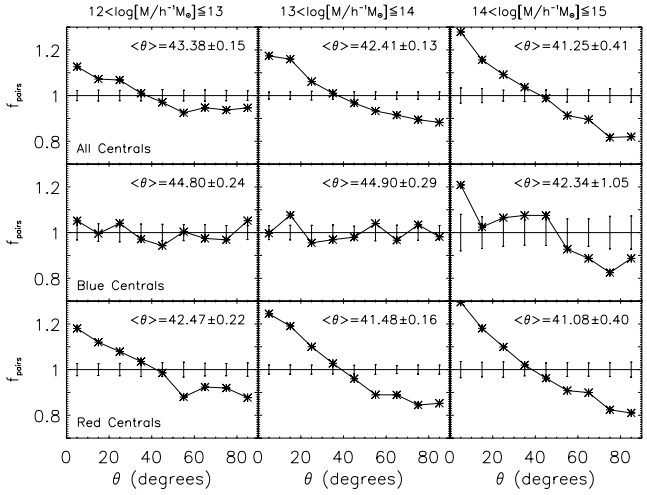

Figure 9. Similar to Fig. 6, but for central-satellite pairs in haloes of different masses as indicated on top of the panels. Results are shown separately for all, red and blue centrals in the upper, middle and lower panels.

$14 \leqslant \log M/h^{-1}\,\mathrm{M}_{\odot} \leqslant 15$, we find no significant alignment signal of satellites with blue centrals. These results are again in good agreement with the findings of Y06 based on galaxy groups in the SDSS DR2 (see also Agustsson & Brainerd 2007).

4.2 The alignment of centrals with their host haloes

As shown above, centrals are aligned with the distribution of their satellite galaxies, and different systems show different levels of alignment. To produce such an alignment signal requires that (i) dark matter haloes are elongated, (ii) satellite galaxies trace the dark matter, at least to some extent, and (iii) the orientation of the central is correlated with the orientation of its dark matter halo. Now that we have obtained constraints on both the shapes of dark matter haloes, we can use the observed alignment signals to constrain the correlation between the orientations of centrals and their dark matter haloes.

Previously, such correlations have been constrained using galaxy catalogues constructed from semianalytical models (SAM) for galaxy formation (see AB06 and K07). In K07, the satellite distributions are modelled using the locations of subhaloes (which are thought to host the satellite galaxies) inside larger dark matter haloes in a numerical simulation. In general, subhaloes are found to be accurate tracers of the shapes of the dark matter distributions of their host haloes. However, since the SAM do not predict the orientations of the centrals, a number of simple assumptions have been made so far, where the minor axis of the central is perfectly aligned with (i) the major axis of the inertia tensor of the host halo, (ii) the minor axis of the inertia tensor of the host halo, (iii) the intermediate axis of the inertia tensor of the host halo or (iv) the angular momentum vector of the host halo. Both AB06 (using the alignment signal measured from isolated host-satellite systems) and K07 (using central-satellite pairs in galaxy groups) found that model (i) predicts an alignment signal that is much too strong compared with the data, model (ii) predicts a strong Holmberg effect, contrary to what is seen and model (iii) predicts almost no alignment. Only model (iv) results in alignment signals that are in agreement with observations. Although this does not give definite proof that the minor axis of the central is perfectly aligned with the angular momentum vector of the halo, it does provide a possible understanding for the origin of a correlation between the orientation a central and that of its host halo.

However, it is important to keep in mind that the SAM not necessarily predict the correct spatial distributions of satellite galaxies. Therefore, in this paper we focus on what can be inferred from the data alone. In particular, we try to *infer*, based purely on the data presented here, to what extent the *projected* orientations of centrals are aligned with those of their dark matter haloes. Similar to what we have done to extract the three-dimensional and two-dimensional axis ratios in Section 3, we compare the data to Monte Carlo simulations. We start from the groups with at least four members, and assume that the projected orientations of the centrals are perfectly aligned with the orientation of the projected satellite distribution. Next, using a Monte Carlo method, we distribute the satellite galaxies according to the projected two-dimensional axis ratios listed in the fourth column of Table 1 for the group sample with $N \geqslant 4$. Finally, we measure the various alignment signals for this Monte Carlo simulation using the same method as described above. The upper panels of Fig. 10 show the alignment signals thus obtained (open symbols) for groups of different masses, as indicated at the top of each panel. For comparison, we also plot the data as asterisks. Clearly, this model predicts an alignment signal that is stronger than observed, especially for the more massive groups.

We can suppress the strength of the alignment signals in the model by taking scatter (i.e. 'random' deviations from perfect alignment) into account. To that extent we assume that the misalignment angle between the projected orientation of the central and the major axis of its host halo can be described by a Gaussian distribution:

$$p(\theta_{\rm mis}) = \frac{1}{\sqrt{2\pi}\sigma} \exp\left(-\frac{\theta_{\rm mis}^2}{2\sigma^2}\right), \tag{10}$$

with σ the standard deviation of the distribution. Note that this distribution for the misalignment angle $\theta_{\rm mis}$ is symmetric and centred around zero.

Using such a Gaussian distribution, we fit the various alignment signals obtained from our SDSS group catalogue, treating σ as a free parameter in each separate case. Here again, we use the minimum χ^2 fit, similar to equation (7) but for the angular distribution of central-satellite pairs (equation 9). The parameter σ is constrained in the range 0°–90°, and on the regular 900 grids. For each σ, the misalignment angles $\theta_{\rm mis}$ are generated according to the Gaussian distributions. We measure the alignment signals in Monte Carlo

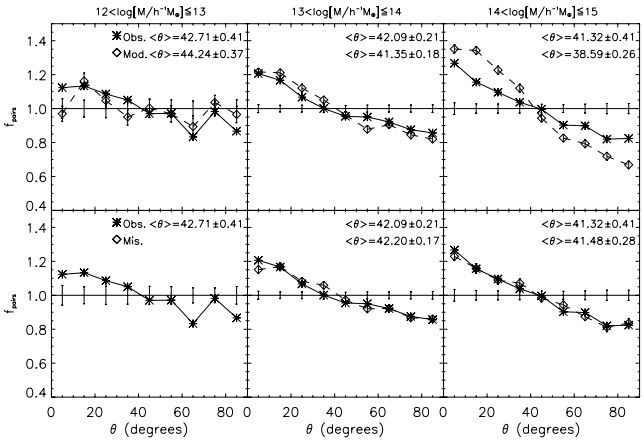

Figure 10. The alignment signal $f_{\rm pairs}(\theta)$ obtained by consider the misalignment angle between the major axis of the dark matter halo and the major axis of the central group galaxy. Upper panels: the alignment signals by assuming that the direction of central is same as the direction of the projected major axis of the dark matter halo (dashed line), comparing to the observed alignment signal (solid line). Lower panels: the comparisons between the observed alignment signal (solid line) and the best-fitting alignment signal by considering a misalignment between the projected major axis of the dark matter halo and the major axis of the central (dashed line).

mock samples in the same way as the observations, and obtain χ^2 values on 900 grids. The best-fitting parameter σ can be obtained from the grid which has the minimum χ^2 value. As an illustration, in the lower panels of Fig. 10 we compare the alignment signals obtained from the data (asterisks) with those obtained from the Monte Carlo simulations including the best-fitting Gaussian distribution of misalignment angles (open symbols). Clearly, the observed results can be well reproduced by such a model. Table 2 lists the best-fitting values of σ thus obtained, for a variety of cases that are shown in Figs 6–9. To better describe these statistical values, 68.3 per cent confidence levels are also given following each best-fitting σ. Here, the confidence levels are obtained from the grids with $\chi^2 = \chi^2_{\rm min} + 1.0$. Clearly, the amount of scatter in the misalignment angle depends strongly on the group mass and the colour of the central. For the entire sample as a whole, we obtain $\sigma \sim 23^\circ$, while groups with red centrals, on average, have smaller misalignment angles than those with blue centrals. Owing to the nearly spherical shapes of dark matter haloes with $12.0 < \log[M/h^{-1}\,{\rm M}_\odot] \leqslant 13.0$, the misalignment angle could not be meaningfully constrained in these cases.

In a recent study, K07 found that if the minor axis of the central and the angular momentum vector of the dark matter halo is in perfect alignment, most of the observational satellite-central alignment signals can be automatically reproduced. On the other hand, any processes that can introduce an average misalignment $\sim 40^\circ$ between the minor axes of central and host dark matter halo can also explain the observed alignment signals. Using high-resolution numerical simulations, Bailin & Steinmetz (2005) found that the angular momentum vectors tend to align with the minor axes of the dark matter halo with a mean misalignment of $\sim 25^\circ$ at small radii and of $\sim 40^\circ$ at the halo virial radius. Here to be able to compare with our findings, as an experiment, we input misalignment angles (with an average $\sim 40^\circ$ and some scatters) between the minor axes of the dark matter haloes and the centrals. By randomly project the three-dimensional shapes of the dark matter haloes and centrals, we measure the distribution of the angles between the *projected major* axes of the dark matter haloes and centrals, if modelled with an Gaussian distribution, which roughly corresponds to $\sigma \sim 22^\circ$. Thus, our finding are in remarkably good agreement with K07 and Bailin & Steinmetz (2005).

Table 2. Best-fitting parameters for the deviation angle between the orientation of the central and the dark matter halo.

Subsample	σ ($^\circ$)
All[a]	$23.3^{+0.1}_{-0.3}$
Blue cen.	$38.1^{+0.1}_{-0.2}$
Red cen.[b]	$16.6^{+0.1}_{-0.1}$
Blue sat.	$29.3^{+0.8}_{-0.1}$
Red sat.[c]	$19.9^{+0.7}_{-0.1}$
Red cen./blue sat.	$38.5^{+0.1}_{-0.6}$
Red cen./red sat.	$16.1^{+0.3}_{-0.1}$
Blue cen./blue sat.	$80.0^{+7.8}_{-21.4}$
Blue cen./red sat.	$37.9^{+0.2}_{-0.1}$
Red cen. (M23[d])	–
Red cen. (M34)	$7.6^{+0.3}_{-0.1}$
Red cen. (M45)	$25.7^{+0.3}_{-0.1}$
Blue cen. (M23)	–
Blue cen. (M34)	$64.8^{+0.1}_{-0.5}$
Blue cen. (M45)	$27.2^{+0.1}_{-0.1}$
All (M23)	–
All (M34)	$23.3^{+0.2}_{-0.3}$
All (M45)	$30.2^{+0.1}_{-0.2}$

[a] All means all centrals.
[b] Blue cen. and Red cen. denote blue centrals and red centrals, respectively.
[c] Blue sat. and Red sat. denote blue satellites and red satellites, respectively.
[d] M23 means that the halo masses are in the range $12 < \log[M/h^{-1}\,{\rm M}_\odot] \leqslant 13$. Note that in M23, the alignment signals for the perfect alignment are already as weak as the observed ones, and so no misalignment angle is introduced.

5 SUMMARY AND DISCUSSION

Using the large galaxy group catalogues constructed from the SDSS Data Release 4 (DR4) by Yang et al. (2007), we have investigated the shapes of their host dark matter haloes, and the correlation between the orientations of the centrals and those of their host haloes. In particular, we obtained the two-dimensional and three-dimensional axis ratios of galaxy groups by comparing the observed, projected ellipticity distributions of satellite galaxies with those of Monte Carlo simulations, and we determined the probability distributions for the angles between the major axis of centrals and the lines connecting the centrals with their satellites. The main results of this paper are summarized as follows.

(i) Under the assumption that the spatial distribution of satellite galaxies traces the shapes of the underlying dark matter haloes, we find that the projected ellipticity distributions are slightly better fit with the triaxial models of JS02 than with simple, spherical NFW models.

(ii) The shapes of dark matter haloes depend strongly on their mass, with more massive haloes being more elongated. Haloes with masses in the range $12 < \log[M/h^{-1}\,\mathrm{M}_\odot] \leqslant 13$ are nearly spherical, while more massive haloes with $14 < \log[M/h^{-1}\,\mathrm{M}_\odot] \leqslant 15$ are more prolate.

(iii) There is no significant difference between the shapes of haloes with red centrals and those with blue centrals.

(iv) Satellites are preferentially distributed along the major axes of their centrals. The strength of this alignment depends strongly on halo mass and on the colours of both central and satellite galaxies. The alignment is strongest between red centrals and red satellites, while blue centrals show almost no alignment at all. More massive groups show a stronger alignment than less massive groups.

(v) The observed alignment can be reproduced if the projected orientation of centrals is aligned with that of the projected mass distribution of its halo. However, the alignment is not perfect. The data can be reproduced under the assumption that the misalignment angle follows a Gaussian distribution around zero, and with a standard deviation of $\sim 23^\circ$. Because of (ii) to (iv), groups with blue centrals have, on average, a larger misalignment angle than those with red centrals.

Our findings regarding the shapes of the galaxy groups are in qualitative agreement with those of P06, and Plionis et al. (2004). However, there are quantitative difference, especially for small haloes. We find that small haloes are almost spherical, and the axis ratios (major to minor) in our measurements are much smaller than their measurements. Note that we have used Monte Carlo simulations to infer the shapes of dark matter haloes, which avoids the impact of selection effects, while in Plionis et al. (2004) the axis ratios are directly measured from the distribution of member galaxies. Although they found that poor groups are more elongated than rich ones, they cautioned that their results may be significantly affected by discreetness effects (see also Plionis et al. 2006). Numerical simulations (e.g. Kasun & Evrard 2005; Allgood et al. 2006) have shown that the small haloes are more spherical than massive haloes, in good agreement with our findings here.

The alignment signals presented here are in good agreement with those obtained by Y06 using a similar, but smaller group catalogue constructed from the SDSS DR2, and with other studies (Brainerd 2005; Agustsson & Brainerd 2006a; Donoso et al. 2006; Agustsson & Brainerd 2007; Azzaro et al. 2007; Faltenbacher et al. 2007a). Contrary to the previous studies by AB06 and K07, our analysis of the implications for the correlation between the orientation of the centrals and that of its halo is based purely on the data presented here, and therefore does not depend on any galaxy formation models or numerical simulations. Nevertheless, tests show that their models of the perfect alignment between the minor axis of the central and angular momentum vector of dark matter halo are in good agreement with our direct measurement of the projected misalignment angles.

ACKNOWLEDGMENTS

We sincerely thank the referee Manolis Plionis for the constructive and detailed comments and suggestions. We also acknowledge helpful discussions with Yipeng Jing, Changbom Park and Xi Kang. This research was supported by the National Science Foundation of China under grants 10373001, 10533010, 10533030, 10673023, 10773001, the Distinguished Young Scholar Grant 10525314, by the Chinese Academy of Sciences under grant KJCX3-SYW-N2, KJCX2-YW-T05, and the *One Hundred Talents* project, by the Shanghai Pujiang Program (No. 07pj14102), by the 973 Program (No. 2007CB815401, 2007CB815402), by the NSF under grant AST-0607535, IIS-0611948 and by the NASA under grant AISR-126270.

REFERENCES

Adelman-McCarthy J. K. et al., 2006, ApJS, 162, 38
Agustsson I., Brainerd T. G., 2006a, ApJ, 644, L25
Agustsson I., Brainerd T. G., 2006b, ApJ, 650, 550 (AB06)
Agustsson I., Brainerd T. G., 2007, American Astron. Soc. Meeting, 211, 09.01
Allgood B., Flores R. A., Primack J. R., Kravtsov A. V., Wechsler R. H., Faltenbascher A., Bullock J. S., 2006, MNRAS, 367, 1781
Altay G., Colberg Jörg M., Croft R. A. C., 2006, MNRAS, 370, 1422
Aragon-Calvo M., van de Weygaert R., Jones B. J. T., van der Hulst T., 2007, ApJ, 655, L5
Aubert D., Pichon C., Colombi S., 2004, MNRAS, 352, 376
Avila-Reese V. et al., 2005, ApJ, 634, 51
Azzaro M., Patiri S. G., Prada F., Zentner A. R., 2007, MNRAS, 376, L43
Bailin J., Steinmetz M., 2005, ApJ, 627, 647
Baldry I. K., Glazebrook K., Brinkmann J., Ivezic Z., Lupton R. H., Nichol R. C., Szalay A. S., 2004, ApJ, 600, 681
Basilakos S., Plionis M., Maddox S. J., 2000, MNRAS, 316, 779
Basilakos S., Plionis M., Yepes G., Gottlöber S., Turchaninov V., 2006, MNRAS, 365, 539
Binggeli B., 1980, A&A, 82, 289
Binggeli B., 1982, A&A, 107, 338
Blanton M. R. et al., 2003, ApJ, 592, 819
Blanton M. R. et al., 2005, AJ, 129, 2562
Brainerd T. G., 2005, ApJ, 628, L101
Brunino R., Trujillo I., Pearce F. R., Thomas P. A., 2007, MNRAS, 375, 184
Bullock J. S., Kolatt T. S., Sigad Y., Somerville R. S., Kravtsov A. V., Klypin A. A., Primack J. R., Dakel A., 2001, MNRAS, 321, 559
Carter D., Metcalfe N., 1980, MNRAS, 191, 325
Ciotti L., Dutta S. N., 1994, MNRAS, 270, 390
Colless M., et al. (The 2dFGRS Team), 2001, MNRAS, 328, 1039
Cooray A., 2000, MNRAS, 313, 783
De Filippis E., Sereno M., Bautz M. W., Longo G., 2005, ApJ, 625, 108
Diemand J., Moore B., Stadel J., 2004, MNRAS, 352, 535
Donoso E., O'Mill A., Lambas D. G., 2006, MNRAS, 369, 479
Einasto M., Einasto J., Müller V., Heinämäki P., Tucker D. L., 2003, A&A, 401, 851
Faltenbacher A., Gottlöber S., Kerscher M., Müller V., 2002, A&A, 395, 1
Faltenbacher A., Li C., Mao S., van der Bosch F. C., Yang X., Jing Y. P., Pasquali A., Mo H. J., 2007a, ApJ, 662, L71
Faltenbacher A., Jing Y. P., Li C., Mao S., Mo H. J., Pasquali A., van der Bosch F. C., 2007b, ApJ, in press (arXiv:0706.0262)
Fasano G., Pisani A., Vio R., Girardi M., 1993, ApJ, 416, 546
Fleck J.-J., Kuhn J. R., 2003, ApJ, 592, 147
Flores R. A., Allgood B., Kravtsov A. V., Primack J. R., Buote D. A., Bullock J. S., 2007, MNRAS, 377, 883
Hahn O., Porciani C., Carollo C. M., Dekel A., 2007a, MNRAS, 375, 489
Hahn O., Carollo C. M., Porciani C., Dekel Avishai., 2007b, MNRAS, 381, 41
Hartwick F. D. A., 1996, in Morrison H., Sarajedini A., eds, ASP Conf. Ser. Vol. 92, Formation of the Galactic Halo . . . Inside and Out. Astron. Soc. Pac., San Franciso, p. 444
Hartwick F. D. A., 2000, AJ, 119, 2248
Hawley D. L., Peebles P. J. E., 1975, AJ, 80, 477
Ho S., Bahcall N., Bode P., 2006, ApJ, 647, 8
Hoekstra H., Yee H. K. C., Gladders Mi. D., 2004, ApJ, 606, 67
Holmberg E., 1969, Ark. Astron., 5, 305
Hopkins P. F., Bahcall N. A., Bode P., 2005, ApJ, 618, 1
Jing Y. P., Suto Y., 2002, ApJ, 574, 538 (JS02)
Kang X., Mao S., Gao L., Jing Y. P., 2005, A&A, 437, 383
Kang X., van den Bosch F. C., Yang X., Mao S., Mo H. J., Li C., Jing Y. P., 2007, MNRAS, 378, 1531 (K07)
Kasun S. F., Evrard A. E., 2005, ApJ, 629, 781

Kazantzidis S., Kravtsov A. V., Zentner A. R., Allgood B., Nagai D., Moore B., 2004, ApJ, 611, L73
Kim R. S. J. et al., (Sloan Digital Sky Survey Collaboration) 2001, A&AS, 199, 142.02
Knebe A., Gill S. P. D., Gibson B. K., Lewis G. F., Ibata R. A., Dopita M. A., 2004, ApJ, 603, 7
Koch A., Grebel E. K., 2006, AJ, 131, 1405
Kroupa P., Theis C., Boily C. M., 2005, A&A, 431, 517
Lee J., 2006, ApJ, 643, 724
Lee J., Suto Y., 2003, ApJ, 585, 151
Lee J., Suto Y., 2004, ApJ, 601, 599
Li C., Kauffmann G., Jing Y. P., White S. D. M., Börner G., Cheng F. Z., 2006, MNRAS, 368, 21
Libeskind N. I., Frenk C. S., Cole S., Helly J. C., Jenkins A., Navarro J. F., Power C., 2005, MNRAS, 363, 146
Lynden-Bell D., 1976, MNRAS, 174, 695
Lynden-Bell D., 1982, Observatory, 102, 202
McConnachie A. W., Irwin M. J., 2006, MNRAS, 365, 902
MacGillivray H. T., Dodd R. J., McNally B. V., Corwin H. G. Jr., 1982, MNRAS, 198, 605
Majewski S. R., 1994, ApJ, 431, L17
Mandelbaum R., Hirata C. M., Broderick T., Seljak U., Brinkmann J., 2006, MNRAS, 370, 1008
Maulbetsch C., Avila-Reese V., Col-n P., Gottlöber S., Khalatyan A., Steinmetz M., 2007, ApJ, 654, 53
Metz M., Kroupa P., Jerjen H., 2007, MNRAS, 374, 1125
Mohr J. J. et al., 1995, ApJ, 447, 8
Navarro J. F., Frenk C. S., White S. D. M., 1996, ApJ, 462, 563
Navarro J. F., Frenk C. S., White S. D. M., 1997, ApJ, 490, 493
Orlov V. V., Petrova A. V., Tarantaev V. G., 2001, MNRAS, 325, 133
Paz D. J., Lambas D. G., Padilla N., Merchán M., 2006, MNRAS, 366, 1503 (P06)
Pereira M. J., Bryan G. L., Gill S. P. D., 2007, preprint (arXiv:0707.1702)
Plionis M., Barrow J. D., Frenk C. S., 1991, MNRAS, 249, 662
Plionis M., Basilakos S., Tovmassian H. M., 2004, MNRAS, 352, 1323 (P04)
Plionis M., Basilakos S., Ragone-Figueroa C., 2006, ApJ, 650, 770
Porciani C., Dekel A., Hoffman Y., 2002, MNRAS, 332, 339
Ragone-Figueroa C., Plionis M., 2007, MNRAS, 377, 1785
Reblinsky K., 2000, A&A, 364, 377
Sales L., Lambas D. G., 2004, MNRAS, 348, 1236
Sales L. V., Navarro J. F., Lambas D. G., White S. D. M., Croton D. J., 2007, MNRAS, 382, 1901
Sereno M., De Filippis E., Longo G., Bautz M. W., 2006, ApJ, 645, 170
Sharp N. A., Lin D. N. C., White S. D. M., 1979, MNRAS, 187, 287
Struble M. F., 1990, AJ, 99, 743
Sulkanen M. E., 1999, ApJ, 522, 59
Tormen G., 1997, MNRAS, 290, 411
Usami M., Fujimoto M., 1997, ApJ, 487, 489
van Haarlem M., van de Weygaert R., 1993, ApJ, 418, 544
Vitvitska M., Klypin A. A., Kravtsov A. V., Wechsler R. H., Primack J. R., Bullock J. S., 2002, ApJ, 581, 799
Wang Y.-G., Fan Z.-H., 2004, ApJ, 617, 847
Wang Y.-G., Fan Z.-H., 2006, ApJ, 643, 630
Wang H. Y., Jing Y. P., Mao S., Kang X., 2005, MNRAS, 364, 424
Weinmann S. M., van den Bosch F. C., Yang X., Mo H. J., 2006, MNRAS, 366, 2
West M. J., 1994, MNRAS, 268, 79
Yang X., Mo H. J., van den Bosch F. C., Jing Y. P., 2005a, MNRAS, 356, 1293
Yang X., Mo H. J., van den Bosch F. C., Weinmann S. M., Li C., Jing Y. P., 2005b, MNRAS, 362, 711
Yang X., van der Bosch F.C., Mo H. J., Mao S., Kang X., Weinmann S. M., Guo Y., Jing Y. P., 2006, MNRAS, 369, 1293 (Y06)
Yang X., Mo H. J., van den Bosch F. C., Pasquali A., Li C., Barden M., 2007, ApJ, 671, 153
Yang X., Mo H. J., van den Bosch F. C., 2008, ApJ, in press (arXiv:0710.5096)
Zaritsky D., Smith R., Frenk C. S., White S. D. M., 1997, ApJ, 478, 53
Zaroubi S., Squires G., Hoffman Y., Silk J., 1998, ApJ, 500, L87
Zaroubi S., Squires G., de Gasperis G., Evrard A. E., Hoffman Y., Silk J., 2001, ApJ, 561, 600
Zehavi I. et al., 2002, ApJ, 571, 172
Zentner A. R., Kravtsov A. V., Gnedin O. Y., Klypin A. A., 2005, ApJ, 629, 219

This paper has been typeset from a TEX/LATEX file prepared by the author.